minerals

MDPI

Article

Flotation Separation of Scheelite from Fluorite Using Sodium Polyacrylate as Inhibitor

Ying Zhang [1,2,*], Youyu Li [1], Rong Chen [2], Yuhua Wang [3,*], Jiushuai Deng [1,2] and Ximei Luo [1,2]

1 State Key Laboratory of Complex Nonferrous Metal Resources Clean Utilization, Kunming 650093, China; 18392020843@163.com (Y.L.); dengshuai689@163.com (J.D.); 85128225@163.com (X.L.)
2 Mineral Processing Engineering, Faculty of Land Resource Engineering, Kumming University of Science and Technology, Kunming 650093, China; 18365403318@163.com
3 Mineral Processing Engineering, School of Minerals Processing and Bio-Engineering, Changsha 410083, China
* Correspondence: zhyingcsu@163.com (Y.Z.); wangyh@mail.csu.edu.cn (Y.W.); Tel.: +86-0871-65187068 (Y.Z.); +86-0731-88830545 (Y.W.)

Academic Editor: Kota Hanumantha Rao
Received: 21 April 2017; Accepted: 14 June 2017; Published: 16 June 2017

Abstract: The depressing properties of sodium polyacrylate (PA-Na) for scheelite and fluorite were studied by micro-flotation tests, infrared spectroscopy (IR), zeta potentials, X-ray photoelectron spectroscopy (XPS), and density functional theory (DFT). The flotation results reveal that the selective depression effect of PA-Na is better than that of sodium silicate, and PA-Na can depress fluorite more effectively than scheelite. The flotation recovery of scheelite and fluorite keeps at about 75% and 10%, respectively, at the pulp pH 9.3~9.6 and PA-Na concentration from 30 to 50 mg/L. IR spectra results suggest that PA-Na has a chemical effect on the surface of scheelite and fluorite. The zeta potential of fluorite becomes more negative than that of scheelite after PA-Na addition. XPS analysis deduces the occurrence of chemisorption between PA-Na and mineral surfaces, and the chemisorption of PA-Na on fluorite is stronger than on scheelite. DFT demonstrates that the absolute value of the adsorption energy in the presence of PA-Na is larger on the fluorite {111} surface than on the scheelite {111} surface. Thus, fluorite is more readily depressed than scheelite, which remarkably matches the micro-flotation test results.

Keywords: scheelite; fluorite; flotation; sodium polyacrylate; selective inhibition

1. Introduction

Scheelite and fluorite are important industrial minerals used as raw materials to produce spaceflight items, catalysts, ceramics, optical glass, and fine chemicals [1]. However, Flotation separation of scheelite from fluorite is difficult because of the existence of the same cation in the minerals and similar physicochemical characteristics such as solubility, hardness, specific gravity, and PZC (point of zero charge) [2]. Flotation techniques have been extensively applied to separate scheelite and fluorite. The traditional scheelite flotation method is the Petrov method [3], which is flotation with high alkalinity, strong stirring, high temperature, high water glass concentration, and high-concentrate pulp. The harsh flotation process conditions make mineral processing an expensive and complex process, and the labor intensity of workers increases [4]. However, scheelite and fluorite have similar surface properties and exhibit high surface reactivity with reagents [5,6]; hence, separating the two minerals is almost impossible without inhibitor addition. In recent years, inhibitors such as organic colloids, sodium phosphates, quebracho, and hydrosols have been used for such a purpose [7,8]; these agents also depress scheelite to a considerable extent. Thus, many scholars continue to study them in order to further strengthen the selective separation of scheelite from fluorite. We tried to find a

more effective inhibitor that can be employed at room temperature. In this study, sodium polyacrylate (PA-Na), an organic inhibitor composed of carboxylic acids, was adopted for the flotation of scheelite and fluorite.

PA-Na is a water-soluble linear polymer. High-molecular-weight PA-Na is used as a flocculant [9–11], whereas the low-molecular-weight form is employed as an inhibitor, dispersant [12], or water-treatment agent [13]. PA-Na is effective only in the flotation of a few sulphide and oxide ores such as lead–zinc sulphide [14], refractory copper oxide [15,16], and lead–zinc oxide ores.

PA-Na is an ideal inhibitor for the flotation separation of scheelite from fluorite. PA-Na is a complex of polyelectrolyte particles and can dissociate into low-molecular-weight ions (Na^+) and polymer ions when the compound is dissolved in an aqueous solution. The polymer ions containing numerous carboxylate ions are multivalent ions. PA-Na is commonly known to depress calcareous gangue by forming a water-soluble complex with the calcium ions (Ca^{2+}) of the mineral surface [17]. The complex would sink to the underflow by the advantages of large quantities of PA-Na, thereby reducing the influence of mineral floatability on collector addition.

In this work, we investigated the flotation of scheelite and fluorite in the absence and presence of PA-Na. The interaction between PA-NA and the minerals was analyzed by infrared spectroscopy (IR). Zeta potential measurements were performed to understand the effects of PA-Na on the surface charges of scheelite and fluorite. X-ray photoelectron spectroscopy (XPS) analysis was employed to determine the binding energy of the interaction between PA-Na and the surface elements. The adsorption energy of PA-Na on the mineral {111} surface was calculated using the density functional theory (DFT), further clarifying the flotation behaviour of minerals by enabling the direct observation of atomic-scale phenomena in complete isolation. On the basis of the above experiments, we chiefly aimed to explain the depressing mechanism of PA-Na adsorption on mineral surfaces.

2. Experimental

2.1. Pure Minerals and Reagents

Pure scheelite was obtained from Ke Muda Mining Ltd. in Tongde County, Qinghai Province, China, and pure fluorite from a mineral powder factory in Changsha, Hunan Province, China. The samples were firstly handpicked, crushed, ground, screened, and finally stored in sealed glass bottles. Elemental analysis showed that the purity of the scheelite and fluorite samples was 94% and 99%, respectively. The particle-size distributions of the samples are displayed in Figure 1. The ground samples were wet-sieved, and −74 μm-sized fractions with specific surface areas of 2533 $cm^2 \cdot g^{-1}$ for scheelite and 2251 $cm^2 \cdot g^{-1}$ for fluorite were collected and used in micro-flotation tests. Some of these particle fractions were further ground in agate mortar to obtain −2 μm particles for zeta potential measurements and XPS analysis.

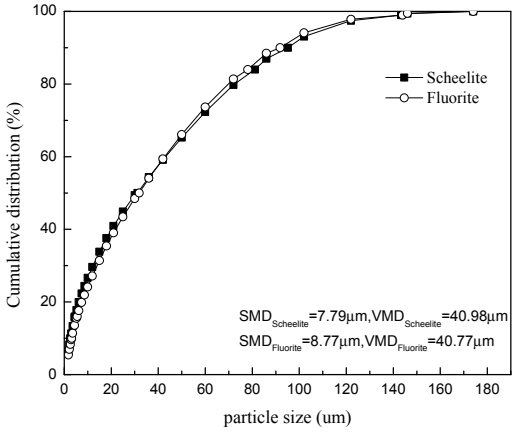

Figure 1. Particle size distribution of the samples.

PA-Na (analytical-reagent grade; Tianjin Kermel Chemical Reagent Co., Ltd., Tianjin, China) was used as the inhibitor; its molecular weight ranges from 800 to 1000 million g/mol. Na_2SiO_3 (analytical-reagent grade; Tianjin Dingshengxin Chemical Industry Co., Ltd., Tianjin, China) is the active ingredient of the water, which is a conventional inhibitor for scheelite flotation. The collector employed was a sodium soap of fatty acids formulated from oxidised paraffin (731), which is an industrial-grade product and is widely applied in scheelite flotation. Sodium carbonate and hydrochloric acid (Tian-heng Chemicals, Tianjin, China) were used to adjust the pH of the pulp. Distilled water was utilized in all the tests unless otherwise specified.

2.2. Micro–Flotation Tests

Flotation tests were carried out in a self-priming trough flotation machine (Figure 2, Jilin Prospecting Machinery Factory, Changchun, China). The volume of the cell is 40 mL, and the rotational speed in the cell was 1650 rpm during flotation. The flotation was conducted as a function of pH in the absence and presence of PA-Na or Na_2SiO_3. The mineral suspension was prepared by adding 3 g of minerals to 40 mL of solutions. The pH of the mineral suspension was adjusted to a desired value by adding Na_2CO_3 or HCl solutions with concentrations of 1% and 2%, respectively, for 2 min. During the tests, the pH of the pulp was measured with a pH meter. The prepared inhibitor and 731 were added at a desired concentration and then conditioned for 3 min. During each flotation test, the froth was collected for a total of 3 min. The dry weights of the concentrate and tail were measured and used to calculate the recovery. Each micro-flotation test was measured three times, and the average was reported as the final value. The standard deviation, which is presented as an error bar, was obtained using the mean of the three measurements per experimental condition. The flotation flowsheet of the experimental procedure of micro-flotation is shown in Figure 3.

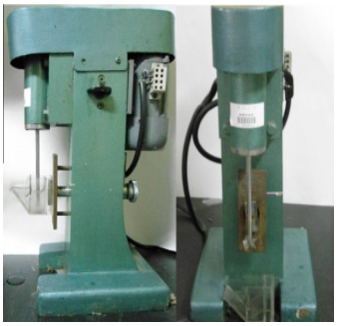

Figure 2. Scheme of flotation machine.

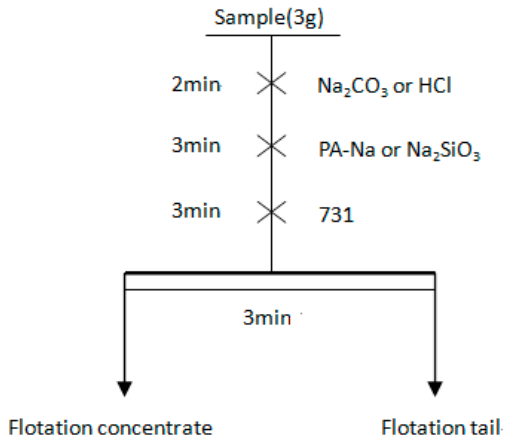

Figure 3. Flotation flowsheet of the experimental procedure of micro-flotation.

2.3. IR Study

For the infrared studies, 1 g pure scheelite or fluorite was individually suspended in 40 mL of reagent solutions for 30 min at pH 9.5. The pulps were then centrifuged and washed at least three times with distilled water and dried in a vacuum oven at 40 °C. The infrared spectra of minerals were recorded using a Model Nexus 670 series Fourier transform infrared spectrometer (Thermo Nicolet Company, Waltham, MA, USA) in the range of 4000–400 cm^{-1}.

2.4. Zeta Potential Measurements

The isoelectric points (IEP) of the mineral samples were determined by measuring the electrophoretic mobility of aqueous dispersions as a function of pH in a zeta potential meter (Beckman Coulter Company, Brea, CA, USA). For these measurements, a mineral dilution suspension was prepared by adding 0.03 g mineral to 50 mL of 10^{-3} M potassium nitrate solution. It was then ultrasonicated for 3 min and then magnetically stirred for 10 min, and the pH was adjusted using Na_2CO_3 or HCl. The zeta potential of the samples was measured using a zeta plus potential meter.

2.5. XPS Analysis

The XPS tests were performed using a K-Alpha 1063 (Physical Electronics, Chanhassen, MN, USA) spectrometer with an Al K_α emission for the X-ray source (operating at 72 W) (Thermo Fisher Scientific, Waltham, MA, USA). A double-gathered and hemi-spherical analyser was employed, with the angle of the sample surface to the analyzer set to 180°. The diameter of the beam spot was 400 μm. The analyzer involved a 128-channel detector with an energy resolution better than 0.5 eV and an error value of 0.3 eV. The samples were mounted on the holder with double-sided tape and transferred to the analysis chamber, in which the vacuum was 10^{-9} mBar. XPS spectra were obtained at room temperature by using PA-Na as an inhibitor. The C 1s value of 284.8 eV was selected as the reference line. Thermo Avantage software was employed to analyse the XPS data [18].

Samples were prepared by adding 1.0 g of pure mineral (<2 μm) and a moderate amount of distilled water in a hitch groove at an effective volume of approximately 40 mL. In accordance with the single-mineral flotation process, we added the reagents, conditioned the mixture for 30 min, and then allowed the mixture to stand for another 30 min. The mixture was subsequently centrifuged for solid–liquid separation, and the sunken fractions were washed twice to thrice with distilled water and then dried in a vacuum oven. Afterwards, the samples were subjected to XPS analysis.

2.6. Computational Details

This study also investigated the competitive adsorption of PA-Na and water on the mineral {111} surface [19]. The surface energy (E_M) of the mineral {111} surface was −37,510.89 eV. The adsorption energy of the adsorbate on the mineral {111} surface was calculated using Equation (1):

$$E_{ads} = E_{M+R} - (E_M + E_R) \quad (1)$$

where E_{M+R} is the energy of the mineral {111} surface with adsorbate molecules; E_M is the energy of the mineral {111} surface; and E_R is the self-energy of the free adsorbate molecule, which is calculated using the same simulation parameters.

In an aqueous environment, the adsorption of PA-Na on the mineral surface was achieved by displacing the pre-adsorbed water on the mineral surface. Consequently, we compared the adsorption energy of PA-Na and water at different modes of adsorption. A negative and lower value indicates that the adsorption of PA-Na with the mineral surface more easily overcomes the resistance of the pre-adsorbed water at the mineral surface. The lowest value was selected for the final evaluation.

Accordingly, the energy values of the adsorption modes of the adsorbate molecule on the mineral {111} surface in the aqueous environment was given by [20,21]:

$$E_{ads} = E_a - E_b \quad (2)$$

where E_{abs} is the final value of adsorption energy. A more negative value of E_{abs} indicates that the adsorption reaction of PA-Na occurs more easily. Specifically, E_a is the adsorption energy of the PA-Na molecule on the mineral surface, and E_b is the adsorption energy of the water molecule on the mineral surface.

The adsorption energy of the adsorbate molecule was calculated using the Cambridge Sequential Total Energy Package (CASTEP) [22,23]. In the CASTEP module, Ultrasoft pseudopotentials were used to represent the interactions between the adsorbate and the minerals. The exchange-correlation energy was determined by a generalised gradient approximation of Perdew-Burke-Ernzerhof (GGA-PBE) [24]. All calculations were performed using a cutoff energy of 340 eV. Reciprocal space integration over the Brillouin zone was approximated with finite sampling of the k-point by using the Monkhorst-Pack scheme, and the k-point spacing was set to 0.04 $Å^{-1}$. The atomic coordinates were optimised using a Broyden-Fletcher-Goldfarb-Shanno scheme, which utilises the total energy and the Hellmann-Feynman forces (<0.05 GPa) on the atoms. The scheme adopted the following thresholds for the converged structure: (a) energy tolerance of 1.0×10^{-5} eV/Å, (b) maximum force tolerance of 0.03 eV/Å, and (c) maximum displacement tolerance of 0.001 Å [25].

3. Results and Discussion

3.1. Single-Mineral Flotation

To compare PA-Na with conventional inhibitor sodium silicate, with 25 mg/L PA-Na or 500 mg/L sodium silicate as an inhibitor and 75 mg/L 731 as a collector, single-mineral flotation of scheelite and fluorite was carried out as a function of pH in the absence and presence of PA-Na or Na_2SiO_3 (Figure 4). With Na_2SiO_3 as the inhibitor, the recovery of scheelite had stable responds at all pH ranges (Figure 4a), but the recovery of fluorite increases as the pH increases (Figure 4b). By contrast, the pH values for the optimum recovery of scheelite and fluorite are different. The flotation recovery of scheelite and fluorite increases slightly as the pH increases and then decreases slightly. The experimental results of scheelite are similar to those reported by Feng [26]. With PA-Na as the inhibitor, the scheelite recovery is about 80.00% in a wide pH range from 8.7 to 10. By contrast, PA-Na exhibits a strong selective depression on fluorite with a maximum recovery of 18.59% at pH 8.2. Na_2SiO_3 has a weak selective depression on the recovery of scheelite and fluorite. Na_2SiO_3 has a certain inhibitory effect on fluorite at pH > 9.5, making the recovery of fluorite reduce by about 10%. With Na_2SiO_3 as the inhibitor, the minimal recoveries of scheelite and fluorite are over 87.56% and 73.42%, respectively. In short, the single-mineral flotation results show PA-Na has a more preferential flotation separation of scheelite from fluorite than Na_2SiO_3 at pulp pH between 8.7 and 10.

The flotation recovery of scheelite and fluorite with 75 mg/L of 731 at the pulp pH 9.3~9.6 as the PA-Na concentration increased is shown in Figure 5. The scheelite floats well with a recovery greater than 75.00%, which is obtained over a wide PA-Na concentration range less than 50 mg/L. When the PA-Na concentration exceeds 50 mg/L, the flotation recovery of scheelite decreases sharply. The flotation recovery of fluorite declines significantly as the PA-Na concentration increases to 30 mg/L. When the PA-Na concentration exceeds 30 mg/L, the flotation recovery of fluorite stabilises at about 10.00%. The preferential flotation separation of scheelite and fluorite is achieved at a pulp pH between 8.7 and 10 and PA-Na concentration between 30 and 50 mg/L (Figures 4 and 5).

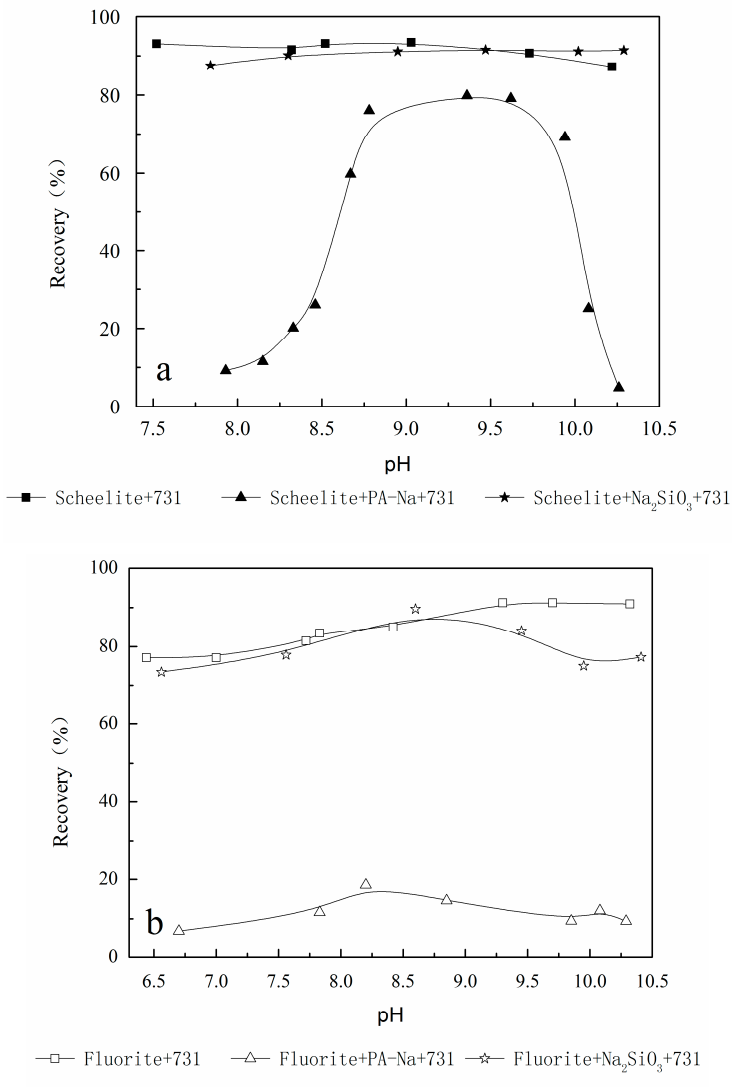

Figure 4. Flotation recovery of scheelite and fluorite as a function of pH in the absence and presence of sodium polyacrylate (PA-Na) or Na_2SiO_3. (**a**)The experimental results of scheelite; (**b**) the experimental results of fluorite.

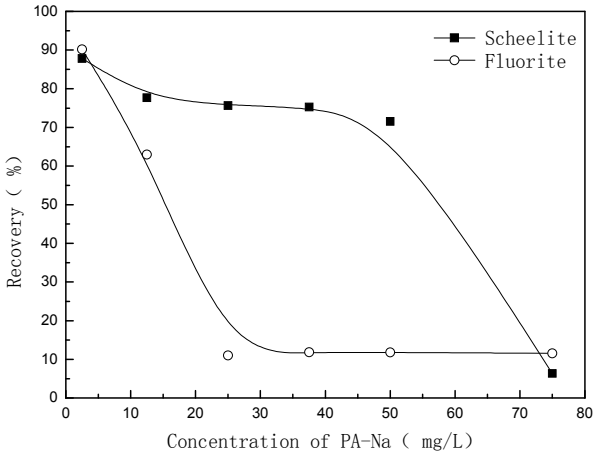

Figure 5. Flotation recovery of scheelite and fluorite as a function of concentration of PA-Na.

3.2. IR Spectra Measurements

According to the IR spectra, it can be determined whether there is a chemical reaction between the reagent and the mineral surface [26]. In order to study the mechanism of Pa-Na in the flotation separation of scheelite from fluorite, the IR (Infrared) spectrums of these two minerals before and after interacting with PA-Na are measured, and the results are shown in Figures 6 and 7.

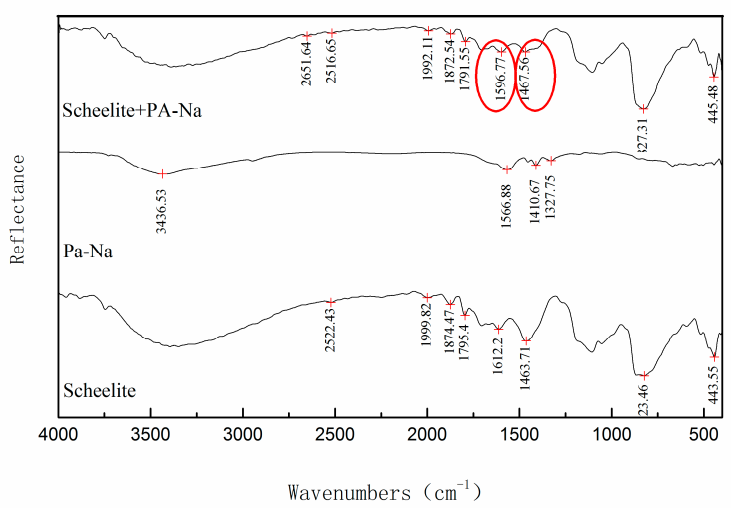

Figure 6. IR (Infrared) spectra of scheelite reacting before and after with PA-Na.

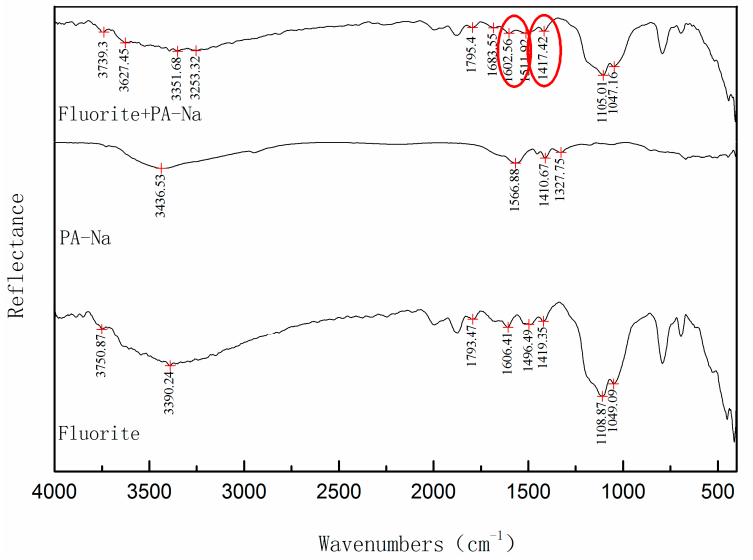

Figure 7. IR spectra of fluorite reacting with PA-Na, before and after.

The IR spectra of scheelite after interacting with PA-Na is shown in Figure 6. According to the literature, there are strong characteristic absorption peaks of COO– in the range of 1580–1530 cm^{-1} wavenumbers, and the weak characteristic absorption peaks of COO– are present in the range of 1420–1375 cm^{-1} wavenumbers [27,28]. The carboxyl groups in sodium polyacrylate were in the form of COO–, forming an asymmetric vibrational absorption peak with a strong intensity near 1564 cm^{-1}, similar to –CH_2–, and a weakly symmetrical vibration near 1410 cm^{-1} [29]. In IR spectra of PA-Na, the anti-symmetrical vibration characteristic peak of the antisymmetric vibrations of carboxylates (COO–) is 1566.88 cm^{-1}. After PA-Na reacting with scheelite, a peak appeared at 1596.77 cm^{-1}, which is the characteristic peak of COO–; the wave number moves by 29.89 cm^{-1} to the higher wave number

and decreases by 15.43 cm^{-1} relative to the surface of the scheelite 1612.2 cm^{-1} absorption peak. The symmetrical vibration characteristic peak at 1410.67 cm^{-1} of PA-Na results in the absorption peak 1467.56 cm^{-1} of scheelite being widened, and the absorption peak at 1463.71 cm^{-1} moves by 3.85 cm^{-1} to the higher wave number. The results illustrate that PA-Na incurs chemisorption on the surface of scheelite.

The IR spectra of fluorite after interacting with PA-Na is shown in Figure 7. After the interaction between fluorite and PA-Na, the peak between 1602.56 and 1511.92 cm^{-1} is relatively flat in a fluorite PA-Na system compared with the peak between 1606.41 and 1496.49 cm^{-1} in a fluorite system. The anti-symmetrical vibration characteristic peak at 1566.88 cm^{-1} of Pa-Na makes the fluorite 1496.49 cm^{-1} peak move to 1511.92 cm^{-1}. Due to the symmetrical vibration characteristic peak at 1410.67 cm^{-1} of Pa-Na, the PA-Na absorption peak at 1419.35 cm^{-1} on fluorite decreases by 1.93 cm^{-1} to a lower wave number of 1417.42 cm^{-1}. The results show that there is a chemical interaction between PA-Na and fluorite.

3.3. Zeta Potential Measurements

Zeta potential measurement is an in situ method used to explore the interactions of ionic species with minerals. In this research, the zeta potentials of scheelite and fluorite pulp were measured in the presence of PA-Na. The pH modifiers were hydrochloric acid and sodium carbonate. The measured zeta potentials for scheelite and fluorite are shown in Figures 8 and 9 respectively.

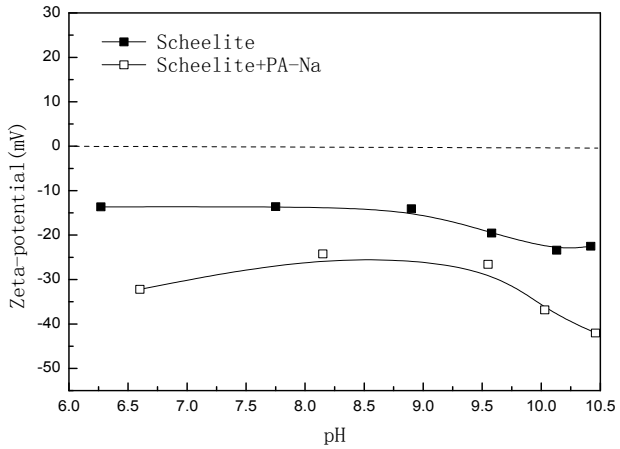

Figure 8. Zeta-potential of scheelite as a function of pH in the absence and presence of PA-Na.

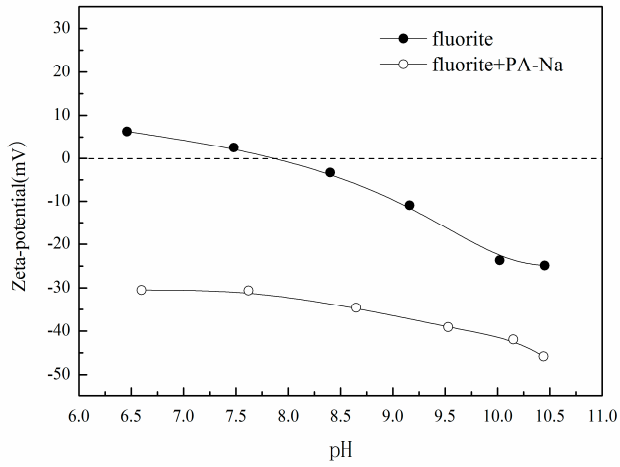

Figure 9. Zeta-potential of fluorite as a function of pH in the absence and presence of PA-Na.

The trends of the zeta potential of scheelite as a function of pH in the absence and presence of PA-Na are shown in Figure 8. Without PA-Na addition (solid symbols), the pH_{IEP} of scheelite do not lie in the pH range between 6 and 10.5. The zeta potential is negative, and values range between −13 and −24, which is similar to the results reported by Gao [30]. The addition of 25 mg/L PA-Na shows a marginal effect on the electrokinetics of scheelite over the pH range in which PA–Na is the dominant species. This effect is considered to be caused by PA-Na adsorbing on the scheelite surface.

As shown in Figure 9, the pH_{IEP} of fluorite is 9.2 without the addition of PA-Na (solid symbols), which is in agreement with previous reports [4]. The addition of 25 mg/L PA-Na causes a significant shift of the IEP to outside the pH range between 6 and 10.5. Such a significant shift in IEP suggests a strong interaction of PA-Na with fluorite, possibly caused by adsorption. Potentiometric titration results [31] show that PA-Na is not dissociated at pH < 4 and is dissociated fully at pH > 9.5; the COO− in the PA-Na are partially dissociated at neutral pH. It is presumed that COO− is dissociated basically at pH > 9; the molecular chain stretching makes a large number of COO− affect the fluorite surface.

PA-Na addition exerts stronger influence on the zeta potentials of fluorite than on those of scheelite over the pH range studied, suggesting a much stronger adsorption of PA-Na on fluorite than on scheelite (Figures 8 and 9). Therefore PA-Na has better inhibitory effect and higher selectivity for fluorite. This observation corresponds well with the much weaker floatability of fluorite than that of scheelite (Figure 4).

3.4. XPS Results

XPS or, alternatively, the electron energy spectrum for chemical analysis, determines the chemical state of an element by measuring the displacement of the inner electron binding energy. This technique is mainly applied for the qualitative analysis of chemical elements, surface element qualitative or semi-quantitative analysis, and chemical valence analysis. XPS is also widely used to study the surface soil layer or super-thin chips such as coatings [32] and nanomaterials [33]; it is applied in the oil chemical field and other industries [34,35].

The atomic compositions of scheelite and fluorite interfaces before and after PA-Na treatment were listed in Table 1. This demonstrates that, after PA-Na adsorption, the atomic concentrations of Ca, C, and O increase and those of W and F decreases by 1.12 and 3.07, respectively, confirming an adsorption of PA-Na onto the two mineral surfaces. In the process of dissolution, scheelite and fluorite will produce a lot of Ca^{2+} ions [36]. The reason may be that Ca^{2+} ions react with PA-Na to form calcium polyacrylate, which can cover the surface of the mineral, so that the concentration of calcium atoms on the mineral surface increases [37]. The results in Table 1 also indicate that the change values of atomic concentration for W, F, C, and O atoms in fluorite are far greater than in scheelite surfaces, which infers that the adsorption amount of PA-Na on fluorite is higher than on scheelite.

Table 1. Atomic concentration of elements for mineral interfaces as determined by X-ray photoelectron spectroscopy (XPS).

Samples	Atomic Concentration of Elements (Atomic %)				
	Ca	W	F	C	O
Scheelite	11.33	18.55	- [b]	26.96	43.16
Scheelite + PA-Na	11.59	17.43	- [b]	27.33	43.65
Δ [a]	0.26	−1.12	- [b]	0.37	0.49
Fluorite	25.37	- [b]	37.17	20.1	17.36
Fluorite + PA-Na	25.58	- [b]	34.1	22.07	18.25
Δ [a]	0.21	- [b]	−3.07	1.97	0.89

[a] Δ is defined as the value of post-treatment minus the value of pre-treatment by PA-Na. [b] is defined as none.

The Ca2p, W 4f, or F 1s XPS of scheelite and fluorite before and after PA-Na treatment are listed in Figures 10 and 11.

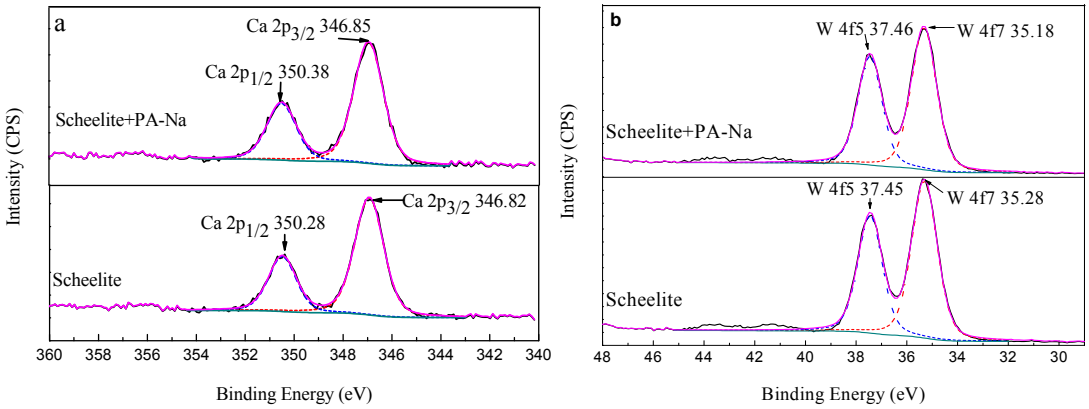

Figure 10. Ca2p or W 4f of scheelite before and after PA-Na treatment. (**a**) Ca2p of scheelite, (**b**) W 4f of scheelite.

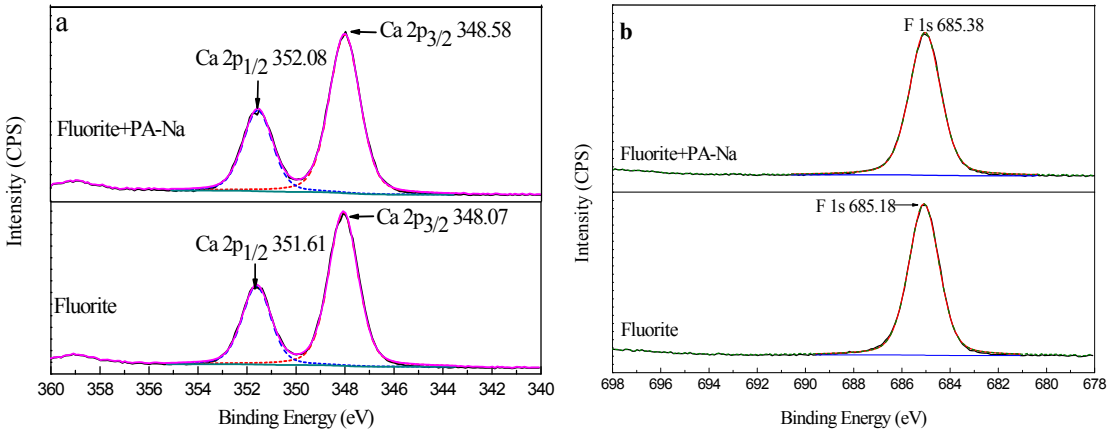

Figure 11. Ca2p or F 1s XPS of fluorite before and after PA-Na treatment. (**a**) Ca2p of fluorite, (**b**) F 1s of fluorite.

The results in Figure 10 illustrate that the changes in the peak intensities of $Ca2p_{3/2}$, $Ca2p_{1/2}$, and W4f may have been induced by PA-Na addition. In the $Ca2p_{3/2}$ and $Ca2p_{1/2}$ spectra, the binding energies of scheelite are 346.82 and 350.28 eV, respectively. After PA-Na addition, the peak position of Ca2p shifts toward a higher binding energy; the binding energies of scheelite increase to 346.85 and 350.38 eV, correspondingly. The binding energies chemically shift by 0.03 and 0.1 eV, respectively (Figure 10a). These findings indicate the presence of a weak force of interaction on the scheelite surface. In the W4f spectra, the binding energy chemically shifts by 0.1 eV and 0.01 eV, respectively, which is less than the experimental error of 0.3 eV (Figure 10b). Thus PA-Na does not influence the $Ca2p_{3/2}$, $Ca2p_{1/2}$, and W4f of the inner electron binding energies of scheelite.

Figure 11 presents the binding energies of the elements in fluorite before and after reacting with PA-Na, and these findings suggest that the changes in the peak intensities of $Ca2p_{3/2}$, $Ca2p_{1/2}$, and F1s are induced by PA-Na addition. The binding energy of the $Ca2p_{3/2}$ peak increases from 348.07 to 348.58 eV, and the binding energy of the $Ca2p_{1/2}$ peak also increases from 351.58 to 352.08 eV, showing corresponding chemical shifts of 0.51 and 0.5 eV, relative to the binding energies before PA-Na addition (Figure 11a). When the chemical shift is greater than the experimental error of 0.3 eV, it indicates that a chemical reaction occurs; the greater the chemical shift, the stronger the reaction [38,39]. The increase in the binding energy of the fluorite surface after PA-Na addition implies the existence of a strong

force of adsorption on fluorite. In the F1s spectra, the chemical shift of the binding energy is 0.2 eV, which is less than the experimental error of 0.3 eV (Figure 11b). Thus, PA-Na significantly affects the Ca2p of the inner electron binding energy of fluorite but does not influence the F1s.

In summary, the XPS tests show that the chemical shift of PA-Na is in the order scheelite << fluorite, suggesting the stronger adsorption PA-Na on fluorite than on scheelite. This finding correlates well with the results of the micro-flotation tests on the chemical adsorption between PA-Na and the mineral surfaces.

3.5. Adsorption Energy

The modes of adsorbate molecule interaction on the mineral {111} surfaces significantly affect the results of the quantum chemical method. The mineral crystal structure and basic unit structure of PA-Na and water are built in a crystal builder module [40,41]. According to the research reports, the magnitude of the adsorption energy can be determined by the form of adsorption and adsorption strength [42]. In other words, if the adsorption is negative, indicating that the adsorption process is exothermic process, the adsorption is stable. The greater the absolute value of the adsorption, the stronger the reaction [43,44]. The modes of PA-Na adsorption on the scheelite {111} surface include the adsorption of the calcium atoms on different electron shells (WP1) and on the same electron shell (WP2). The modes of H_2O adsorption on the scheelite {111} surface involve adsorption on the top of the oxygen atom (WH1), on the two oxygen atoms of a single tungstate group (WH2), and on the two oxygen atoms from different tungstate groups (WH3).

A detailed description of the comparison between the sorption of PA-Na and the pre-adsorbed water is presented in Tables 2 and 3. The adsorption energies are listed in Table 2, which provides insights into the adsorption energies of the adsorbates to the scheelite {111} surface; the adsorption energy of the calcium atoms on the same electron shell (WP2) is −359.27 kJ/mol lower than that of the calcium atoms on different electron shells (WP1). These results denote that the adsorption between PA-Na and the scheelite {111} surface involves chemisorption. The adsorption energy of the water molecules is the lowest at the mode of WH2; the energy value is −225.70 kJ/mol, indicating a strong adsorption between the water molecules and the scheelite {111} surface.

Table 2. Adsorption energy of PA-Na and water on the scheelite {111} surface.

Mineral	Mode of Adsorption	$E_{(M+R)}$ (eV)	E_M (eV)	E_R (eV)	E_{ads} (eV)	E_{ads} (KJ/mol)
Scheelite + PA-Na	WP1	−42,915.93	−37,510.89	−5401.65	−3.39	−327.21
	WP2	−42,916.26	−37,510.89	−5401.65	−3.76	−359.27
Scheelite + H_2O	WH1	−37,978.42	−37,510.89	−467.20	−0.32	−31.27
	WH2	−37,980.43	−37,510.89	−467.20	−2.34	−225.70
	WH3	−37,979.35	−37,510.89	−467.20	−2.26	−121.50

Table 3. Adsorption energy of PA-Na and water on the fluorite {111} surface.

Mineral	Mode of Adsorption	$E_{(M+R)}$ (eV)	E_M (eV)	E_R (eV)	E_{ads} (eV)	E_{ads} (KJ/mol)
Fluorite + PA-Na	FP1	−14,714.07	−9310.34	−5399.82	−3.91	−376.62
	FP2	−14,714.37	−9310.34	−5399.82	−4.20	−405.32
Fluorite + H_2O	FH1	−9777.70	−9310.34	−466.82	−0.55	−52.96
	FH2	−9777.31	−9310.34	−466.82	−1.155	−111.41
	FH3	−9777.32	−9310.34	−466.82	−1.162	−112.03

The mode of PA-Na adsorption on the fluorite {111} surface includes the adsorption of calcium atoms on different shells (FP1) and on the same shell (FP2). The mode of water-molecule adsorption on the fluorite {111} surface involves the adsorption on the top of fluorine (FH1), on the two fluorine atoms of the same electron shell (FH2), and on the two fluorine atoms of different electron shells (FH3).

The adsorption energy of PA-Na on the fluorite {111} surface is shown in Table 4. The adsorption energy of PA-Na is −405.32 kJ/mol at the mode of FP2, which is lower than that on the calcium atom of different electron shells (FP1). This finding demonstrates that the adsorption between PA-Na and the fluorite {111} surface involves chemisorption. The determination of the adsorption energy of the water molecules shows that FH2 and FH3 attained nearly similar adsorption energies at −111.41 and −112.03 kJ/mol, respectively.

Table 4. The adsorption energy of PA-Na adsorbing on the mineral {111} surface in an aqueous environment (KJ/mol).

Mode of Adsorption	E_b	Mode of Adsorption	E_a	E_{ads}
Scheelite + H_2O	−225.70	Scheelite + PA-Na	−359.27	−133.57
Fluorite + H_2O	−112.03	Fluorite + PA-Na	−405.32	−293.29

The adsorption energy of PA-Na in an aqueous environment is calculated using Equation (2), and the results are listed in Table 4. The results for E_{abs} are negative, and the adsorption energy of PA-Na on fluorite in the aqueous environment is lower than on scheelite, confirming that PA-Na exhibits better selectivity for fluorite than for scheelite. This result is consistent with the results of the micro-flotation tests.

4. Conclusions

In this paper, PA-Na was used as an inhibitor for the selective depression of scheelite and fluorite. The flotation performance and mechanism for the separation of scheelite and fluorite were evaluated by micro-flotation tests, zeta potential, XPS, and DFT computation. Based on the experimental results, the following conclusions can be drawn:

The micro-flotation results demonstrate that the selective depression of PA-Na is stronger than that of sodium silicate. PA-Na exhibits superior depressing performance for fluorite and a weak depressing capacity for scheelite. With the use of PA-Na as an inhibitor at its optimum concentration range from 30 to 50 mg/L, scheelite can be floated well over a pulp pH range between 8.7 and 10, whereas fluorite can be depressed at the same pH values.

The results of IR spectra, zeta potential, XPS, and DFT computation illustrate that there is stronger chemisorption of PA-Na on fluorite than on scheelite. The addition of PA-Na displays more distinct electrokinetics in fluorite than in scheelite. In an aqueous environment, the absolute value of the adsorption energy of PA-Na on fluorite is higher than that on scheelite, confirming that PA-Na exhibits better selectivity for fluorite than for scheelite. This investigation of mechanism is consistent with the results of the micro-flotation tests.

Acknowledgments: This work was financially supported by the National Natural Science Foundation of China (No. 51504108, 51404119 and 51604130).

Author Contributions: Ying Zhang and Yuhua Wang conceived and designed the experiments; Ying Zhang, Youyu Li and Rong Chen performed the experiments; Ying Zhang, Jiushuai Deng and Ximei Luo analyzed the data; Ying Zhang contributed reagents/materials/analysis tools; Ying Zhang and Youyu Li wrote the paper.

Conflicts of Interest: The authors declare no conflict of interest.

References

1. Atademir, M.R.; Kitchener, J.A.; Shergold, H.L. The surface chemistry and flotation of scheelite, II. Flotation "collectors". *Int. J. Miner. Process.* **1981**, *8*, 9–16. [CrossRef]
2. Gao, Z.Y.; Bai, D.; Sun, W.; Cao, X.F.; Hu, Y.H. Selective flotation of scheelite from calcite and fluorite using a collector mixture. *Miner. Eng.* **2015**, *72*, 23–26. [CrossRef]

3. Han, H.S.; Hu, Y.H.; Sun, W.; Li, X.D.; Cao, C.G.; Liu, R.Q.; Yue, T.; Meng, X.S.; Guo, Y.Z.; Wang, J.J.; et al. Fatty acid flotation versus BHA flotation of tungsten minerals and their performance in flotation practice. *Int. J. Miner. Process.* **2017**, *159*, 22–29. [CrossRef]
4. Gao, Z.W.; Zheng, C.H.; Zhang, Z.R.; Xin, B.J. Experimental Study of Scheelite Flotation at Room Temperature. *China Tungsten Ind.* **2010**, *25*, 18–20. (In Chinese).
5. Gao, Z.Y.; Gao, Y.S.; Zhu, Y.Y.; Hu, Y.H.; Sun, W. Selective Flotation of Calcite from Fluorite: A Novel Reagent Schedule. *Minerals* **2016**, *6*, 114. [CrossRef]
6. Zhang, Y.; Wang, Y.H.; Li, S.L. Flotation separation of calcareous minerals using dido-decyldimethylammonium chloride as a collector. *Int. J. Min. Sci. Technol.* **2012**, *22*, 285–288. [CrossRef]
7. Feng, B.; Guo, W.; Xu, H.G. The combined effect of lead ion and sodium silicate in the flotation separation of scheelite from calcite. *Sep. Sci. Technol.* **2017**, *52*, 567–573. [CrossRef]
8. Yin, W.Z.; Wang, J.Z.; Sun, Z.M. Structure-activity relationship and mechanisms of reagents used in scheelite flotation. Rare. *Rare Met.* **2015**, *34*, 882–887. [CrossRef]
9. Lu, Y.P.; Zhong, H.; Huang, X.H. Flotation of fine wolframite flocs using polyacaylic acid as flocculant: Its mechanism. *Min. Met. Eng.* **1994**, *14*, 37–41. (In Chinese)
10. Wang, Y.H.; Huang, C.B.; Hu, Y.H.; Hu, Y.M.; Lan, Y. Beneficiation of diasporic—Bauxite ore by selective flocculation with a polyacrylate flocculant. *Miner. Eng.* **2008**, *21*, 664–672. [CrossRef]
11. Huang, C.B.; Zhang, L.; Wang, Y.H.; Lan, Y. Separation of aluminosilicates and diaspore from diasporic-bauxite by selective flocculation. *J. Cent. South Univ. Technol.* **2008**, *15*, 520–525. [CrossRef]
12. Rubio, J.; Marabini, A.M. Factors affecting the selective flocculation of hydroxyl apatite from quartz and/or calcite mixtures. *Int. J. Miner. Process.* **1987**, *20*, 59–71. [CrossRef]
13. Guerrero, L.; Omil, F.; Méndez, R.; Lema, J.M. Protein recovery during the overall treatment of wastewaters from fish-meal factories. *Bioresour. Technol.* **1998**, *63*, 221–229. [CrossRef]
14. Silvestre, M.O.; Pereira, C.A.; Gallery, R.; Peres, A.E.C. Dispersion effect on a lead–zinc sulphide ore flotation. *Miner. Eng.* **2009**, *22*, 752–758. [CrossRef]
15. Qi, D.D.; Li, Z.H.; Hu, X.G. Studies on the separation of chalcopyrite from galena using polyacrylate sodium. *Min. Met. Eng.* **1991**, *11*, 32–34. (In Chinese)
16. Yang, X.W.; Sheng, J.H.; Da, C.S.; Wang, H.S.; Su, W.; Wang, R.; Chan, A.S. Polymer-Supported BINOL Ligand for the Titanium-Catalyzed Diethylzinc Addition to Aldehydes: A Remarkable Positive Influence of the Support on the Enantioselectivity of the Catalyst. *J. Org. Chem.* **2000**, *65*, 295–296. [CrossRef] [PubMed]
17. Bulatovic, S.M. *Handbook of Flotation Reagents: Chemistry Theory and Practice*; Elsevier Science & Technology: Amsterdam, The Netherlands, 2007; p. 25.
18. Sun, W.; Tang, H.H.; Chen, C. Solution chemistry behavior of sodium silicate in flotation of fluorite and scheelite. *Chin. J. Nonferr. Met.* **2013**, *23*, 2274–2283.
19. Cooper, T.G.; de Leeuw, N.H. A computer modeling study of the competitive adsorption of water and organic surfactants at the surfaces of the mineral scheelite. *Langmuir* **2004**, *20*, 3984–3994. [CrossRef] [PubMed]
20. De Leeuw, N.H.; Cooper, T.G. The layering effect of water on the structure of scheelite. *Phys. Chem. Chem. Phys.* **2003**, *5*, 433–436. [CrossRef]
21. Rai, B.; Rao, T.K.; Krishnamurthy, S.; Vetrivel, R.; Mielczarski, J.; Cases, J.M. Molecular modeling of interactions of diphosphonic acid based surfactants with calcium minerals. *Langmuir* **2002**, *18*, 932–940. [CrossRef]
22. Payne, M.C.; Teter, M.P.; Allan, D.C.; Arias, T.A.; Joannopoulos, J.D. Iterative minimization techniques for abinitio total-energy calculations: Molecular dynamics and conjugate gradients. *Rev. Mod. Phys.* **1992**, *64*, 1045–1097. [CrossRef]
23. Zhao, G.; Zhong, H.; Qiu, X.Y.; Wang, S.; Gao, Y.D.; Dai, Z.L.; Huang, J.P.; Liu, G.Y. The DFT study of cyclohexyl hydroxamic acid as a collector in scheelite flotation. *Miner. Eng.* **2013**, *49*, 54–60. [CrossRef]
24. Perdew, J.; Burke, P.K.; Ernzerhof, M. Generalized gradient approximation made simple. *Phys. Rev. Lett.* **1996**, *77*, 3865–3868. [CrossRef] [PubMed]
25. Gao, Z.Y.; Sun, W.; Hu, Y.H. Surface energies and appearances of commonly exposed surface of scheelite crystal. *Trans. Nonferr. Met. Soc. China* **2013**, *23*, 2147–2152. [CrossRef]
26. Feng, B.; Luo, X.P.; Wang, J.Q.; Wang, P.C. The flotation separation of scheelite from calcite using acidified sodium silicate as depressant. *Miner. Eng.* **2015**, *80*, 45–49.

27. Taylor, J.J.; Sigmund, W.M. Adsorption of sodium polyacrylate in high solids loading calcium carbonate slurries. *J. Colloid Interface Sci.* **2010**, *341*, 298–302. [CrossRef] [PubMed]
28. Bigi, A.; Boanini, E.; Borghi, M.; Cojazzi, G.; Panzavolta, S.; Roveri, N. Synthesis and hydrolysis of octacalcium phosphate: Effect of sodium polyacrylate. *J. Inorg. Biochem.* **1999**, *75*, 145–151. [CrossRef]
29. Parida, S.K.; Dash, S.; Patel, S.; Mishra, B.K. Adsorption of organic molecules on silica surface. *Adv. Colloid. Interface Sci.* **2006**, *121*, 77–110. [CrossRef] [PubMed]
30. Gao, Y.S.; Gao, Z.Y.; Sun, W.; Hu, Y.H. Selective flotation of scheelite from calcite: A novel reagent scheme. *Int. J. Miner. Process.* **2016**, *154*, 10–15. [CrossRef]
31. Drzymala, J.; Fuerstenan, D.W. Selective F1occulation of Hematite in the Hematite-Quartz-Ferric Ion-Polyacrylic Acid System, Part I, Activation and Deactivation of Qaartz. *Int. J. Miner. Process.* **1981**, *7*, 258.
32. Wallenhorst, L.M.; Loewenthal, L.; Avramidis, G.; Gerhard, C.; Militz, H.; Ohms, G.; Viöl, W. Topographic, optical and chemical properties of zinc particle coatings deposited by means of atmospheric pressure plasma. *Appl. Surf. Sci.* **2017**, *410*, 485–493. [CrossRef]
33. Alinauskas, L.; Brooke, E.; Regoutz, A.; Katelnikovas, A.; Raudonis, R.; Yitzchaik, S.; Payne, D.J.; Garskaite, E. Nanostructuring of SnO_2 via solution-based and hard template assisted method. *Thin Solid Films* **2017**, *626*, 38–45. [CrossRef]
34. Lei, Z.W.; Zhang, G.Z.; Deng, Y.H.; Wang, C.Y. Surface modification of melamine sponges for pH-responsive oil absorption and desorption. *Appl. Surf. Sci.* **2017**, *416*, 798–804. [CrossRef]
35. Konstantin, I.M.; Yury, A.T.; Sergey, V.S.; Stepan, N.K.; Anton, Y.T.; Kirill, E.I. XPS study of Uranium-Containing sodium-Aluminum-Iron-Phosphate glasses. *J. Alloy. Compd.* **2017**, *712*, 560–566.
36. Wang, D.Z.; Hu, Y.H. *Solution Chemistry of Flotation*; Hunan Science and Technology Press: Changsha, China, 1988. (In Chinese)
37. Ylikantola, A.; Linnanto, J.; Knuutinen, J.; Oravilahti, A.; Toivakka, M. Molecular modeling studies of interactions between sodium polyacrylate polymer and calcite surface. *Appl. Surf. Sci.* **2013**, *276*, 43–52. [CrossRef]
38. Moreira, G.F.; Peçanha, E.R.; Monte, M.B.M.; Filho, L.S.L.; Stavale, F. XPS study on the mechanism of starch-Hematite surface chemical complexation. *Miner. Eng.* **2017**, *110*, 96–103. [CrossRef]
39. Parasyuk, O.V.; Khyzhun, O.Y.; Piasecki, M.; Kityk, I.V.; Lakshminarayana, G.; Luzhnyi, I.; Fochuk, P.M.; Fedorchuk, A.O.; Levkovets, S.I.; Yurchenko, O.M.; et al. Synthesis, structural, X-ray photoelectron spectroscopy (XPS) studies and IR induced anisotropy of Tl4HgI6 single crystals. *Mater. Chem. Phys.* **2017**, *187*, 156–163. [CrossRef]
40. Hu, Y.H.; Gao, Z.Y.; Sun, W.; Liu, X.W. Anisotropic surface energies and adsorption behaviors of scheelite crystal. *Colloids Surf. A Phys. Eng. Asp.* **2012**, *415*, 439–448. [CrossRef]
41. Zhang, Y.; Wang, Y.H.; Hu, Y.H.; Wen, S.M.; Wang, J.M. First-Principe Theory Calculation of Electronic Structures of Scheelite, Fluorite and Calcite. *Chin. J. Rare Met.* **2014**, *38*, 1106–1113. (In Chinese)
42. Hu, H.P.; Wang, M.; Ding, Z.Y.; Ji, G.F. FT-IR, XPS and DFT Study of the Adsorption Mechanism of Sodium Salicylate onto Goethite or Hematite. *Acta. Phys. Chim. Sin.* **2016**, *32*, 2059–2068.
43. Yang, X.L.; Liu, S.; Liu, G.Y.; Zhong, H. A DFT study on the structure–reactivity relationship of aliphatic oxime derivatives as copper chelating agents and malachite flotation collectors. *J. Ind. Eng. Chem.* **2017**, *46*, 404–415. [CrossRef]
44. Deng, J.S.; Lei, Y.H.; Wen, S.M.; Chen, Z.X. Modeling interactions between ethyl xanthate and Cu/Fe ions using DFT/B3LYP approach. *Int. J. Miner. Process.* **2015**, *140*, 43–49. [CrossRef]